Nanoscale

Accepted Manuscript

This article can be cited before page numbers have been issued, to do this please use: A. Hannecart, D. Stanicki, L. Vander Elst, R. N. Muller, S. Lecommandoux, J. Thévenot, C. Bonduelle, A. Trotier, P. Massot,

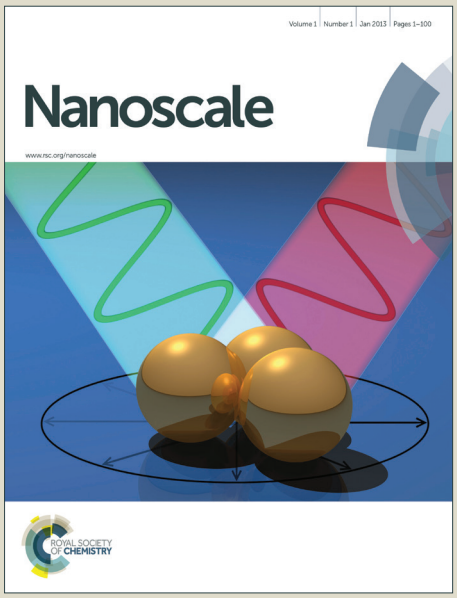

ROYAL SOCIETY OF CHEMISTRY

www.rsc.org/nanoscale

View Article Online
DOI: 10.1039/C4NR07064J

Cite this: DOI: 10.1039/c0xx00000x

www.rsc.org/xxxxxx

PAPER

Nano-thermometer with Thermo-sensitive Polymer Grafted USPIOs behaving as Positive Contrast Agents in low-field MRI

Adeline Hannecart,[a] Dimitri Stanicki,[a] Luce Vander Elst,[a,b] Robert N. Muller,[a,b] Sébastien Lecommandoux,[c] Julie Thévenot,[c] Colin Bonduelle,[c] Aurélien Trotier,[d] Philippe Massot,[d] Sylvain Miraux,[d] Olivier Sandre,*[c] and Sophie Laurent*[a,b]

Received (in XXX, XXX) Xth XXXXXXXXX 20XX, Accepted Xth XXXXXXXXX 20XX
DOI: 10.1039/b000000x

Two commercial statistical copolymers of ethylene oxide and propylene oxide, Jeffamine® M-2005 (PEO_5-*st*-PPO_{37}) and M-2070 (PEO_{46}-*st*-PPO_{13}), exhibiting lower critical solution temperature (LCST) in water, were grafted onto the surface of ultra-small superparamagnetic iron oxide nanoparticles (USPIOs) using silanization and amide-bond coupling reactions. The LCSTs of the polymers in solution were measured by dynamic light scattering (DLS) and nuclear magnetic resonance (NMR). In accordance with the compositions of EO *vs.* PO, the transition temperature was measured at 22±2°C for M-2005 both by DLS and NMR, while the LCST was much higher, 52±2°C, for M-2070 (a second transition being also detected above 80°C by NMR in that case, ascribed to the full dehydration of chains at molecular level). The resulting polymer-grafted USPIOs exhibit a temperature-responsive colloidal behaviour, their surface reversibly changing from hydrophilic below LCST to hydrophobic above it. This phenomenon was utilised to design thermo-sensitive contrast agents for MRI. Transverse relaxivities (r_2) of the USPIO@PEO_5-*st*-PPO_{37} core-shell nanoparticles were measured at 8.25, 20, 60, and 300 MHz. Nuclear magnetic resonance dispersion (NMRD) profiles, giving longitudinal relaxivities (r_1) between 0.01 and 60 MHz, were acquired at temperatures ranging from 15 to 50°C. For all tested frequencies except 300 MHz, both r_1 and r_2 decrease with temperature and show an inflection point at 25°C, near the LCST. To illustrate the interest of such polymer-coated USPIOs for MRI thermometry, sample tubes were imaged on both low-field (8.25 MHz/0.194 Tesla) and high-field (300 MHz / 7.05 Tesla) MRI scanners with either T_1- or T_2^*-weighted spin echo sequences. The positive contrast on low-field MR images and the perfect linearity of the signal with a T_2^*-weighted sequence over the whole temperature range 15°C – 50°C render these LCST polymer coated USPIOs interesting positive contrast agents, also working as "nano-thermometers".

Introduction

Superparamagnetic iron oxide nanoparticles are widely studied due to their unique properties such as high magnetisation, biocompatibility and biodegradability.[1] Their main biomedical application is their use as contrast agents for magnetic resonance imaging (MRI).[2] Iron oxide nanoparticles lead to a MRI contrast enhancement by accelerating the relaxation of magnetic moments of water protons. The efficiency of a MRI contrast agent is quantified by its relaxivities r_1 and r_2, defined as the increases of the proton nuclear relaxation rates $1/T_1$ and $1/T_2$ of the solvent brought by one millimole of equivalent iron per liter ($s^{-1}\cdot mM_{Fe}^{-1}$), respectively for longitudinal (r_1) and transverse (r_2) relaxations. Superparamagnetic iron oxide nanoparticles are divided into ultra-small (USPIO) monocrystalline cores with hydrodynamic diameters (D_h) below 40 nm and polycrystalline clusters denoted SPIOs. The clustering of several magnetic cores usually leads to a high r_2/r_1 ratio that can reach values up to several hundred depending on magnetic field (Larmor frequency) of the MRI scanner. Thus SPIOs are mostly used with T_2 or T_2^*-weighted MR pulse sequences, introducing a "negative contrast" on images, *i.e.* appearing darker than the pure buffer or tissue. However, very small diameter USPIOs maintaining a low r_2/r_1 ratio (typically less than 3-4) can also act as "positive contrast agents" (appearing brighter than pure water) as long as they stay individually dispersed in the suspension, *i.e.* their hydrodynamic diameters remain low, *e.g.* D_h<20 nm.[3,4] This implies that not only magnetic cores are small, but also that they are protected from aggregation by a repulsive shell. This stabilising coating can be made of the hydrophilic biocompatible polymer poly(ethyleneglycol) either as a homopolymer[3] or a copolymer block,[4] but other biopolymers like glycopolypeptides were also reported to prevent clustering and obtain efficient positive (T_1) contrast agents.[5]

To grow a dense polymer brush at the surface of USPIOs, a "grafting on" technique is usually preferred to simple polymer adsorption, which rather leads to multi-core clusters generating

View Article Online
DOI: 10.1039/C4NR07084J

hypo-signals on MR images like for the commercial negative (T_2) contrast agent Endorem®. Thus one needs first to introduce functions for further coupling reactions, by grafting covalently a monolayer of short and densely packed organic molecules such as (3-aminopropyl)triethoxysilane (APTS), a molecule frequently used in the literature to introduce amino groups.[5,6] Instead of working on bare hydrophilic USPIOs, certain studies start with a ligand-organosilane exchange on hydrophobic USPIOs initially coated by oleic acid.[7,8] Even though the surface modification of iron oxide nanoparticles with APTS only is not sufficient to achieve colloidal stability at pH 7 in high salinity buffers, it is often a first step to further functionalise the USPIOs with longer molecules.[5,6] Other functionalities were introduced by grafting organosilanes at the surface of USPIOs for various coupling reactions, like epoxide[4] or cyanide[9], or a brominated endgroup as initiator for controlled radical polymerisation.[8]

Besides preventing aggregation of the USPIOs, the presence of a non-magnetic shell wrapping the magnetic cores can also directly influence the r_1 and r_2 relaxivities if it is impermeable to water. For example, a significant decrease of r_1 and r_2 with the coating thickness was observed for silica shells synthesised by a sol-gel method.[10] On the contrary, a highly hydrated shell around densely clustered USPIOs like in magnetic hydrogels can greatly enhance the r_2 relaxivity up to 500-600 $s^{-1}\cdot mM_{Fe}^{-1}$.[11] The so-called "outer sphere" model describes all these behaviours and enables predicting the r_2 value in the high field of most clinical imagers through a unified scaling law with three parameters only: the distance of closest approach between water protons and the centre of the superparamagnetic particle (R_{NMR}), the intra-particle volume fraction of magnetic materials (Φ_{intra}) and the magnetisation (defined as the volume concentration of magnetic moments) at saturation (M_S) of the whole sphere:[12]

$$r_2 \cdot \Phi_{intra} = \gamma^2 \mu_0^2 \, v_{mol} \left(M_S \cdot R_{NMR} \right)^2 / 405 \, D \qquad (1)$$

$\gamma \approx 2.67513\times10^8$ rad·s^{-1}·T^{-1} being the proton gyromagnetic factor, $\mu_0 = 4\pi10^{-7}$ T·m·A^{-1} the magnetic permeability of vacuum, D the diffusion constant of water molecules, and v_{mol} the specific volume of the magnetic material, ~15.7 cm^3·mol^{-1} for iron oxide. This formula is valid only in the so-called "Motional Averaging Regime", *i.e.* in a limited range of size and magnetisation values. Above this limit, the transverse relaxivity reaches a maximum described by the "Static Dephasing Regime" that cannot be easily compared to experimental data without the use of numerical simulations.[12]

This work reports the grafting of thermo-sensitive Jeffamine® M-2005 and M-2070 onto the surface of iron oxide nanoparticles. Jeffamine® products are amino-terminated statistical copolymers of ethylene oxide (EO) and propylene oxide (PO) units. These commercial poly(ether)amines exhibit a lower critical solution temperature (LCST) in water: soluble in water below the LCST, they undergo a reversible coil-to-globule transition at the LCST and become insoluble at temperatures above the LCST.[13] Several systems proposed in the literature took benefit of both this temperature-dependant water solubility of Jeffamine® and of its primary amine end-group, enabling further functionalisation. Block copolymers of Jeffamine® M-2005 with a polypeptide[14] or a polysaccharide[15] are soluble in water below the LCST and form self-assembled structures above it. Co-adsorption onto magnetic core-silica shell nanoparticles of a diblock copolymer of Jeffamine® M-2005 with poly(*L*-lysine) (PLL) and PLL-*b*-PEO enabled forming a polymer corona eliciting a LCST tuneable by the PO content.[16] In another study, M-1000, M-2070 and M-2005 Jeffamine® poly(ether)monoamines were grafted onto carboxylated cellulose nanocrystals by amide bond formation.[17]

The grafting of Jeffamine® onto iron oxide nanoparticles was also described, using epoxide ring opening by the primary amine group of M-1000 and M-2070.[4] The resulting polymer brushes around the USPIOs were dense and repulsive, and provided good colloidal stability to the nanocrystals, as shown by their positive contrast agent behaviour on MRI images,[4] ascribed to a low r_2/r_1 ratio. The longitudinal and transverse relaxivities were reported in this work, but not their variation with temperature, presumably because M-1000 and M-2070 are very hydrophilic (their LCST is too high). On the contrary, the higher PO content of M-2005 ensures that its LCST is just above room temperature. Therefore it is well adapted to study how r_1 and r_2 relaxivities of iron oxide nanoparticles vary when their surface changes from hydrophilic to hydrophobic, for a given magnetic core size and magnetisation.

The effect of a thermo-sensitive polymer coating on the proton relaxivities of USPIOs was reported in literature in the case of poly(*N*-isopropylacryamide) (PNIPAM), a widely used polymer with a LCST of 32°C. At 60 MHz, r_1 decreased above the LCST whereas r_2 increased, so that r_2/r_1 increased a lot, as a result of USPIOs' clustering when their coating became hydrophobic.[22] In a control experiment with a purely hydrophilic PEO coating, r_2 decreased and r_1 remained almost constant as temperature rose.[22] In another work on USPIOs dispersed in water through a bilayer of surfactants (thus impermeable to water), a similar rather weak variation of r_1 with temperature was described (with a slope whose sign was dependent upon USPIOs' size), whereas the trend of r_2 when raising temperature was always a strong decrease.[23]

The present work aims at deciphering the effect of a polymer corona dehydration above LCST on r_1 and r_2 as sketched on Scheme 1, while keeping the USPIOs in a dispersed state (thus a low r_2/r_1 ratio), and examining the results on the MR images with T_1-weighted and T_2^*-weighted spin echo sequences.

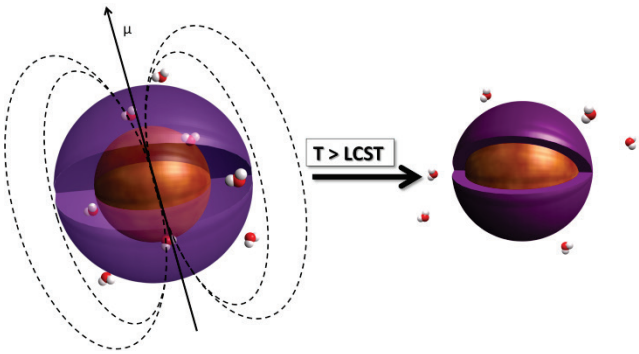

Scheme 1 Sketch of an ultrasmall superparamagnetic iron oxide (USPIO) core wrapped by a thermo-sensitive polymer shell (in purple) highly hydrated below the LCST that becomes impermeable to water molecules above it. The magnetic moment μ and the field lines are also represented.

Experimental Section

Synthesis of iron oxide nanoparticles

Iron oxide nanoparticles were synthesised in high temperature

View Article Online
DOI: 10.1039/C4NR07064J

polyol medium by alkaline coprecipitation of $FeCl_2$ and $FeCl_3$ under optimised parameters.[18] A mixture of $FeCl_2$ (45 mmol) and $FeCl_3$ (37 mmol) (nFe^{II}/nFe^{III}=1.22) in diethyleneglycol (250 mL) was first mixed (150 rpm) and heated at 170°C under nitrogen flux (1.5 mL·min^{-1}). After 15 min, NaOH (15 g) was added to the medium, which was stirred during 1 h at 170°C. After cooling to room temperature, the black precipitate was isolated from the solution by magnetic decantation and washed five times with HNO_3 1M (200 mL). After readily dispersion of the nanoparticles in 100 mL of de-ionised (DI) water, the suspension was stirred overnight. Finally, the magnetite nanoparticles were sonicated for 45 min and centrifugated at 16770 g for 45 min to pellet any un-dispersed solid.

Surface functionalisation with carboxylic groups

The iron oxide nanoparticles were functionalised by reaction of their surface hydroxyls with 3-triethoxysilylpropyl succinic anhydride (TEPSA), an organosilane used as precursor of carboxylic acids. Briefly, 50 mL of DMF was added to 20 mL of the aqueous suspension of nanoparticles (~16 mmol iron). Water was then eliminated by evaporation under reduced pressure. After cooling to room temperature, 4.3 mL of DI water, 7.1 mL of TEPSA (28 mmol) and 2.5 mL of tetramethylammonium hydroxide 1 M (2.5 mmol) were added to the suspension. The reaction mixture was heated at 100°C for approximately 40 h. After cooling to room temperature, the iron oxide nanoparticles were precipitated by an acetone/ether mixture (50/50, 300 mL) and washed two times with acetone (100 mL). The suspension was finally dispersed in 100 mL of DI water and washed by ultra-filtration with ultrapure water. The iron concentration 0.156 mol$_{Fe}$·L^{-1} was measured accurately by T_1 relaxometry at 20 MHz after mineralisation of the nanoparticles into ferric ions. The COOH moieties were titrated by conductimetry, yielding a molar ratio of 2.8 mol% acidic functions compared to total iron content.

Coating with poly(ether)monoamines by "grafting on"

Jeffamine® M-2005 and M-2070 were gifts from Huntsman, The Netherlands. Their compositions in EO and PO units and molar masses were checked by ^{1}H NMR, respectively PEO_5-*st*-PPO_{37} (2400 g·mol^{-1}) for M-2005 and PEO_{46}-*st*-PPO_{13} (2800 g·mol^{-1}) for M-2070. The amines were titrated by perchloric acid in 1:2 (v/v) chloroform / glacial acetic acid, yielding 97±2 % NH_2 end-groups for the two poly(ether)amine batches. The two Jeffamine® polymers were grafted covalently onto TEPSA-coated iron oxide nanoparticles using carbodiimide (EDC) to activate the carboxylate groups of TEPSA. The conditions of the coupling reaction were found optimal at pH 6 with molar ratios $n_{poly(ether)amine}/n_{TEPSA}$=12.5 and n_{EDC}/n_{TEPSA}=10. Briefly, 26 mL of phosphate buffer (pH 6) containing 0.52 g of Jeffamine® M-2005 (220 µmol) or 0.62 g of Jeffamine® M-2070 (220 µmol) were added to 4 mL of Fe_3O_4-TEPSA nanoparticles suspension (624 µmol$_{Fe}$, 17.5 µmol$_{COOH}$). To start the coupling reaction, 33.5 mg of EDC (175 µmol) were added. The mixture was stirred for 18 h below the LCST, *i.e.* at 4°C for Jeffamine® M-2005 and at room temperature for M-2070. Finally, un-grafted chains were removed through dialysis for approximately 72 h with 10 bath changes. Alternatively, the grafted suspension was diluted 20 times in DI water and then concentrated again by ultra-filtration under a nitrogen pressure across a regenerated cellulose membrane of pore size smaller than the USPIOs (30000 g·mol^{-1} molecular weight cut-off) until no trace of polymer was detected by FT-IR in the ultra-filtrate after freeze-drying.

Instrumentation

Dynamic light scattering (DLS) and phase analysis light scattering (PALS) were conducted on a Zetasizer NanoZS ZEN 3600 instrument (Malvern, UK) to measure the hydrodynamic diameters (D_h), polydispersity index (PDI) and ζ potential of the nanoparticles. The measurements were performed in dilute suspensions in pure water, *i.e.* 16 g·L^{-1} for the polymer chains and around 1 mM$_{Fe}$ (0.08 g·L^{-1}) for the USPIOs of different coatings. Reported D_h and PDI values were measured in triplicate from the 2nd order cumulant fit of the correlograms obtained from scattered light intensity at 173°.

Nuclear magnetic relaxation dispersion (NMRD) profiles reporting the longitudinal relaxation rates of water protons (R_1) over a magnetic field range from 0.24 mT to 0.94 T were recorded on a Fast Field Cycling Relaxometer (Stelar, Mede, Italy). Additional longitudinal (R_1) and transverse (R_2) relaxation rates were measured at 0.47 T and 1.41 T on Minispec mq20 and mq60 relaxometers (Bruker, Karlsruhe, Germany). The saturation magnetisation, M_S, and size of superparamagnetic crystals, R_{NMR}, were determined by fitting these NMRD curves numerically with the MINUIT minimisation program within the frame of the Outer Sphere model and a standard phenomenological approximation.[19]

Iron concentration was determined by longitudinal relaxation rate (R_1) measurements at 0.47 T and 37°C after microwave digestion (MLS-1200 MEGA, Milestone) into ferric ions by a mixture of nitric acid and hydrogen peroxide.[20]

Fourier transform infrared (FT-IR) transmission spectra were recorded in the range 450-4000 cm^{-1} through the samples dispersed in KBr pellets on a Spectrum 100 FT-spectrometer (Perkin Elmer, US).

Nuclear magnetic resonance (NMR) spectra were recorded on a Bruker Avance 500 MHz spectrometer (Karlsruhe, Germany). Temperature was adjusted by an air flow or a liquid nitrogen flow controlled by a Bruker BVT 3200 unit. 90° pulse and an acquisition delay of 1 s were used for ^{1}H spectral accumulations.

Thermogravimetric analyses (TGA) were conducted on a TA Q500 system (TA Instruments). Before analysis, the samples were first heated at 80°C during 24 h to eliminate free water. The mass loss of the pre-dried samples was monitored under nitrogen from room temperature to 120°C at a heating rate of 10°C/min. After an isotherm at 120°C under nitrogen during 10 min to remove the bound water, the samples were heated from 120°C to 600°C at a heating rate of 10°C/min under air.

Low-field MR images of sample tubes were acquired on a Siemens Magnetom open magnet clinical scanner at 0.194 T (8.25 MHz). T_1-weighted images were taken with a spin-echo sequence of *TR*=100 ms, *TE*=2.8 ms, 70° flip angle. T_2^*-weighted images were taken with *TR*=300 ms, *TE*=12 ms, 160×160 mm^2 field of view, 128×128 matrix, 7 mm slice thickness. The apparent transverse relaxation rates $R_2^*=1/T_2^*$ at 8.25 MHz were measured for a series of six samples at increasing concentrations (0.05, 0.1, 0.25, 0.5, 0.75, and 1 mM$_{Fe}$) with a Carr Purcell Meiboom Gill (CPMG)-like sequence made of 16 echoes with 12 ms inter echo-time. For all MRI experiments, the samples in 2 mL vials were placed in a water jacket of temperature controlled

View Article Online
DOI: 10.1039/C4NR07084J

by a regulated circulating bath (Huber Polystat CC, Offenburg, Germany). Temperature was monitored inside the chamber in the magnet by a GaAs-based optical fibre thermometer compatible with radiofrequency magnetic fields (Opsens, Québec, Canada).

High-field MR images were taken on a Bruker PharmScan 70/16 for small animal imaging with a 7.05 T magnet (300 MHz) with spin-echo sequences of *TR*=1000 ms, *TE*=8.5 ms, 25.6×25.6 mm^2 field of view, 256×256 matrix, and 2 mm slice thickness. Relaxivities at 7.05 T were measured on a Bruker Avance 300.

Results and Discussion

Solution properties of the poly(ether)amine chains

The LCST values of Jeffamine® M-2005 and M-2070 were determined by two different methods, DLS intensity and NMR spectroscopy. The cloud points of the two polymer solutions at 16 $g \cdot L^{-1}$ in H_2O were measured by following the backscattered intensity at 173°: the inflection points were respectively near 22±2°C and 52±2°C for Jeffamine® M-2005 and M-2070 (Fig. 1). In the meanwhile, the liquid state proton NMR signal of the polymer backbone fell down above the LCST, because of a globular state analogous to a solid state.[21] The ^1H spectra of the poly(ether)amine solutions at 30 $g \cdot L^{-1}$ in D_2O were recorded at increasing temperatures (Fig. S1 in Supporting Information). Fig. 1 shows the steep signal decrease when temperature exceeded 25°C for M-2005: the curve of NMR signal appeared almost symmetrical to the plot of DLS intensity. In the case of M-2070, the drop of NMR signal was only 10% above 55°C. However a weak inflection symmetrical to the DLS curve can still be identified as a sign of the LCST. But it is only above 80°C that the NMR signal started to decrease significantly. We interpret this apparent discrepancy by the sensitivity of DLS to the onset of the transition when the very first clusters of polymer globules started to aggregate (and then sediment, causing a slight decrease of the DLS intensity, as seen at 35°C for M-2005 and 65°C for M-2070). On the contrary, the ^1H NMR intensity probes the local environment of the chains that became fully dehydrated at a high temperature than the LCST. Nevertheless, the inflection point of the curves provides a good determination of the LCST for both polymers with both techniques.

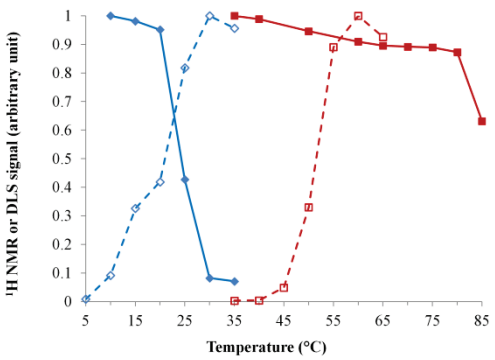

Fig. 1 Normalised area under the ^1H NMR spectrum (filled markers, solid lines) and derived count-rate in DLS (empty markers, dotted lines) *vs.* temperature for Jeffamine® M-2005 (blue) and M-2070 (red) at 16 $mg \cdot mL^{-1}$ in H_2O for DLS and 30 $mg \cdot mL^{-1}$ in D_2O for NMR. The LCST is determined at the inflections points of both curves, 22±2°C for M-2005, 52±2°C for M-2070 (in that case a second transition above 80°C is visible by NMR, corresponding to full dehydration of the chains).

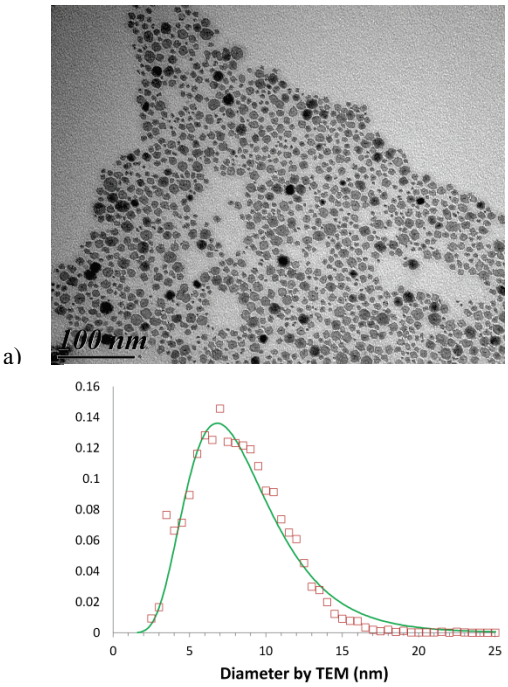

Fig. 2 a) TEM image of Jeffamine® M-2005 coated-USPIOs (scale bar 100 nm) and b) histogram of TEM diameters deduced by automatic particle counting (red square) on five images with a total number of 7950 nanoparticles, and fitted by a log-normal law (green line) of parameters d_0=8 nm and σ=0.4.

Characterisation of the organic coating of the nanoparticles

The organic shell composed of a first TEPSA organosilane layer, then the polymer, was analysed by FT-IR spectroscopy (Fig. S2 and S4), TGA (Table 1, Fig. S3), DLS and zetametry (Fig. 3).

At first, the FT-IR spectrum of USPIOs synthesised by alkaline coprecipitation of $FeCl_2$ and $FeCl_3$ in DEG medium (Fig. S2a) contains bands at 591 and 635 cm^{-1} originating from Fe-O stretching of the Fe_3O_4 cores. The narrow peak at 1384 cm^{-1} is ascribed to nitrate ions physisorbed on iron oxide surface. The spectrum also contains a band at 1630 cm^{-1} due to water physisorbed on iron oxide surface and a broad band around 3400 cm^{-1} due to surface hydroxyl groups (Fe-OH).

The FT-IR spectrum of USPIOs grafted with TEPSA (Fig. S2b) shows a band at 1119 cm^{-1} characteristic of Si-O bonds. The band at 2925 cm^{-1} originates from C–H stretching of CH_2 groups. The bands at 1711, 1560 and 1404 cm^{-1} are assigned to carboxylates. As a result, the presence of a TEPSA layer on the iron oxide surface was confirmed by infrared spectroscopy.

Table 1 Weight compositions of hybrid USPIOs measured by TGA

Sample (coating)	Bound water (wt. %)	Inorganics =Iron oxide (wt. %)	Total organics = (wt. %)	TEPSA + (wt. %)	Polymer (wt. %)
TEPSA coated	2.7[a]	87.5[a]	12.5[a]	12.5[a]	0
		100[b]	14.3[b]	14.3[b]	
M-2005 coated	1.4[a]	60.1[a]	39.9[a]	8.6[a]	31.3[a]
		100[b]	66.4[b]	14.3[b]	52.1[b]
M-2070 coated	1.6[a]	77.8[a]	22.2[a]	11.1[a]	11.1[a]
		100[b]	28.5[b]	14.3[b]	14.2[b]

[a] relatively to dry matter at 120°C; [b] ratio to burnt matter at 600°C.

To quantify this layer, an organic-to-inorganic ratio of 14.3%

View Article Online
DOI: 10.1039/C4NR07064J

was determined from the weight loss on the TGA curve of the TEPSA-coated USPIOs (Fig. S3). We deduced the number n_{TEPSA} of organosilane molecules grafted to the USPIO nanoparticle by:

$$\frac{\text{organic wt.\%}}{\text{inorganic wt.\%}} = \frac{n_{TEPSA} \times M_w^{TEPSA}}{M_w^{USPIO}} \quad (2)$$

with the molar mass of particle M_w^{USPIO} estimated geometrically:

$$M_w^{USPIO} = \rho \times N_A \times \frac{4}{3}\pi r_{USPIO}^3 \quad (3)$$

where N_A is the Avogadro number and ρ the mass density of Fe_3O_4, ρ=5180 kg·m^{-3}. Using r_{USPIO}=5.5 nm as determined later by relaxometry (R_{NMR}), one finds $M_w^{USPIO} \approx 2\times10^6$ g·mol^{-1}. Since M_w^{TEPSA}=304.4 g·mol^{-1}, the number of molecules in the coating is $n_{TEPSA} \approx 1000$ molecules per nanoparticle, covering an area $4\pi\times(r_{USPIO})^2 \approx 380$ nm^2. From these values, a surface density of 2.6 TEPSA molecules per nm^2 is estimated, in accordance with values reported in the literature for silane monolayers on ferrite nanoparticles.[7]

For USPIO nanoparticles firstly coated with TEPSA then coupled to Jeffamine® chains, the organic content measured by TGA is the sum of the two components:

$$\frac{\text{organic wt.\%}}{\text{inorganic wt.\%}} = \frac{n_{TEPSA} \times M_w^{TEPSA}}{M_w^{USPIO}} + \frac{n_{polymer} \times M_w^{polymer}}{M_w^{USPIO}} \quad (4)$$

The grafting density of the silane being *a priori* not affected by the coupling reaction of the polymer, the weight ratio of TEPSA relatively to Fe_3O_4 can be considered constant (14.3 wt.%) for all samples. With this hypothesis of constant TEPSA-to-iron-oxide weight fraction, the first term of this sum can be subtracted from the left hand of Eq. (4) (total organic-to-inorganic content), yielding the fraction of polymer relatively to inorganic weight (Table 1). Finally, this polymer-to-inorganic ratio enables to estimate the number of chains per USPIO: $n_{polymer} \approx 430$ chains per USPIO for Jeffamine® M-2005 ($M_w^{polymer}$=2400 g·mol^{-1}), and $n_{polymer} \approx 100$ chains for M-2070 ($M_w^{polymer}$=2800 g·mol^{-1}). The yields of the chain coupling were thus respectively 43% and 10%.

The grafting of Jeffamine® onto the surface of USPIOs was also studied by FT-IR spectroscopy. Unfortunately, the amide bond formation between the carboxylic acid of TEPSA and the amino group of Jeffamine® could not be detected directly on the raw spectra, since the C=O vibration was expected to overlap the wide band between 1550 and 1700 cm^{-1} of USPIOs coated by TEPSA only (Fig. S2b). To highlight the presence of amide bands, the two FT-IR spectra of USPIOs coated with TEPSA respectively before and after the grafting of Jeffamine® were first normalised relatively to iron oxide by setting the same absorption of the Fe-O bond in the 450–600 cm^{-1} range. Then they were subtracted and plotted in the 1000–2000 cm^{-1} wave number range (Fig. S4a for M-2005 and Fig. S5a for M-2070). The resulting spectrum shows three bands ascribed to carbonyl groups (red circle), two in the 1650–1690 cm^{-1} range for amide carbonyle groups (amide band I for C=O, amide band II for N-H) and one characteristic of the remaining carboxylic acids (1730 cm^{-1}). The other bands at lower wave numbers (one near 1455 cm^{-1}, four bands between 1400 and 1250 cm^{-1} and one band near 1100 cm^{-1}, blue circles) were typical of poly(ether)amines, as compared to the spectra of the pure polymers (respectively Fig. S4b and S5b). The coupling of the amino-terminated polymers with the carboxylic acids of the organosilane coating on the iron oxide surface was thus proven undoubtedly.

Colloidal behaviour of the grafted nanoparticles

The colloidal state of the suspensions was probed by dynamic and phase analysis light scattering techniques. Fig. 3 shows the ζ potential of the raw, the TEPSA-coated and Jeffamine®-coated USPIOs followed by PALS *vs.* pH to locate their point of zero charge (PZC). The hydrodynamic diameters were taken as the intensity-average diameters measured by DLS. Dispersed in dilute HNO_3 medium, the bare USPIOs exhibit a D_h=14.3±0.2 nm (PDI=0.13). After grafting of TEPSA, D_h became equal to 18.0±0.1 nm (PDI=0.13). Values measured again after 1 month did not vary significantly. In addition to this increase of D_h by about 4 nm between coated and un-coated USPIOs, the organic and highly hydrated shell was also attested by the plot of the ζ potential as a function of pH (Fig. 3). The PZC was initially at pH 5.8, a typical value for iron oxide. After grafting with TEPSA, the PZC was shifted to pH≈3. The USPIO nanoparticles became stable on a much wider range of pH, *i.e.* for pH higher than 4.5. Deprotonated above this pH, the carboxylic acid functions of TEPSA provide strong enough electrostatic repulsion to prevent the aggregation of the USPIOs, as seen from a strongly negative ζ potential (-30 mV at pH 4.5, and -40 mV above pH 6 with fully deprotonated carboxylates).

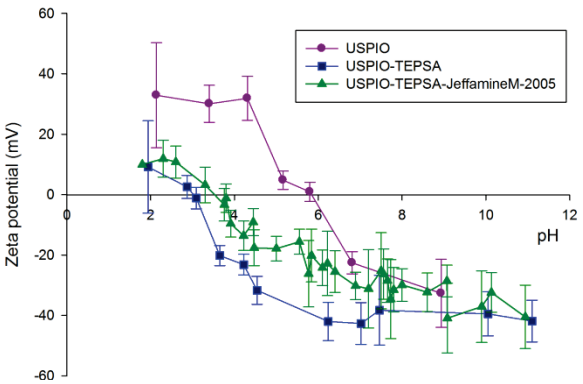

Fig. 3 Evolution of ζ potential of the raw iron oxide nanoparticles after coprecipitation (purple circles), after coating with TEPSA (blue squares) and after grafting of Jeffamine® M-2005 (green triangles) *vs.* pH. The error bars represent the experimental uncertainty of the PALS method for each data point, which increases towards lower or higher pH due to the increased salinity forcing to lower the voltage to 50 V instead of 150 V.

The curve of ζ potential *vs.* pH for the polymer-coated nanocrystals was slightly shifted towards higher pH values compared to the silane-coated ones. This phenomenon is ascribed to partial hydrodynamic screening of the negative charges of the remaining carboxylates groups by the polymer chains. Negative ζ potential values with a PZC in the range pH=4.5–5 was already reported in the literature for poly(ether)amine coated-USPIOs and was explained by residual surface charges arising from the organosilane layer, in that case deprotonated hydroxyl groups.[4]

View Article Online
DOI: 10.1039/C4NR07084J

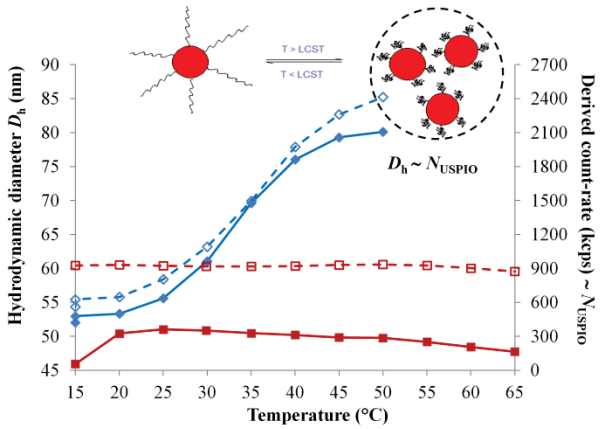

Fig. 4 Intensity-average hydrodynamic diameter D_h (nm, filled markers, solid lines) and derived count-rate in DLS (empty markers, dotted lines) *vs.* temperature for USPIOs grafted with Jeffamine® M-2005 (blue) and M-2070 (red). The measurements were performed at 1 mM_{Fe} in water. The grafting of M-2005 chains formed USPIOs clusters of size and aggregation number both increasing with temperature, whereas TEPSA-coated USPIOs remained individually dispersed over the whole *T*-range.

The hydrodynamic size (D_h, PDI) and the scattered intensity of the USPIOs grafted with Jeffamine® chains were followed by DLS as a function of temperature at pH 6 in the range 15-65°C (Fig. 4). At 15°C, the hydrodynamic sizes were respectively D_h=52 nm (PDI=0.07) for the USPIOs grafted with Jeffamine® M-2005 and D_h=46 nm (PDI=0.26) for those grafted with Jeffamine® M-2070. The intensity scattered by the particles and their sizes (calculated at each temperature with the appropriate value of water viscosity) appeared constant for USPIOs grafted with the most hydrophilic chains, Jeffamine® M-2070 up to 65°C, in agreement with the weaker grafting density (yield of the chain coupling = 10%) and/or an incomplete dehydration of the polymer chains below 80°C. On the contrary, the colloidal state highly depends on temperature for USPIOs grafted with Jeffamine® M-2005 (LCST of the chains in solution at 22±2°C). Both D_h and the scattered intensity exhibited an increase with a sigmoid shape in the 15–50 °C range. Apparently, the two sigmoid curves can be superposed on a double-axis plot (Fig. 4), meaning a proportionality factor between them. The clusters of USPIOs were thus rather tenuous (low Φ_{intra}), since the number of USPIOs per aggregate (proportional to the scattered intensity) would have varied rather with the power 3 of D_h for dense clusters, whereas here it varied linearly with the cluster size. This information is important to interpret the relaxometric properties later on.

Relaxometric properties of LCST polymer-coated USPIOs

Relaxivities of the USPIO nanoparticles grafted with polymers were studied as a function of temperature for both Jeffamine® batches. But in view of its lower LCST, the results are emphasised for M-2005, the relaxometric data for M-2070 being given as controls in supporting information (Fig. S6 and S7). While r_1 was obtained as a function of frequency using Fast Field Cycling relaxometry, r_2 was measured at discrete frequencies relevant for clinical MRI scanners: 8.25, 20, 60 and 300 MHz.

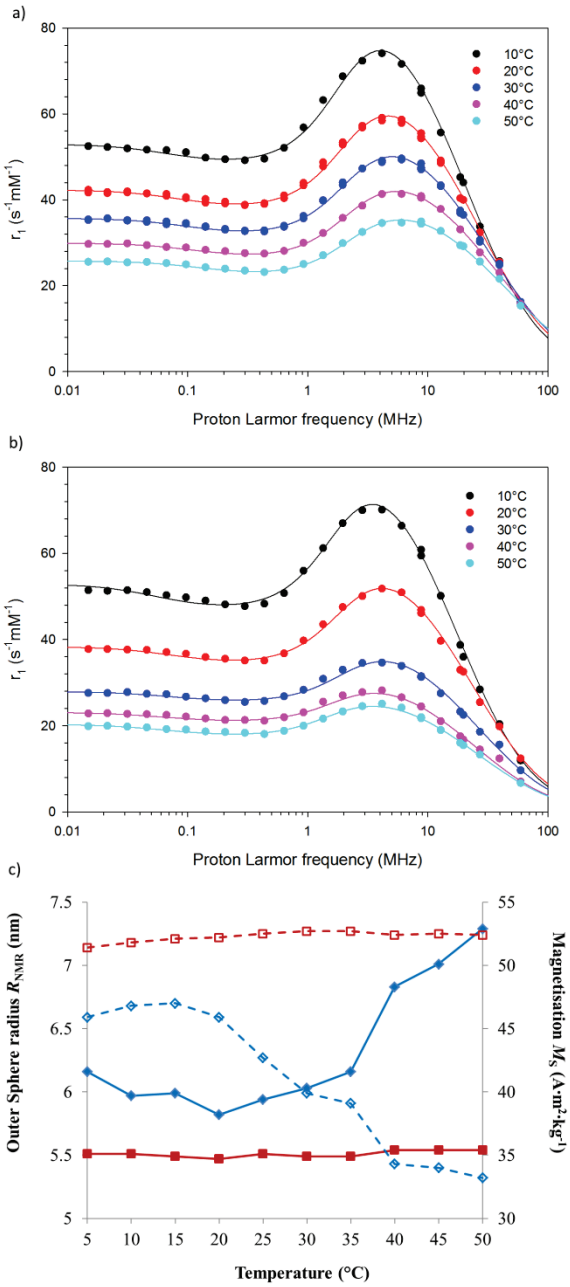

Fig. 5 NMRD profiles of the longitudinal relaxivity *vs.* Larmor frequency for a) TEPSA-coated USPIOs, and b) USPIOs grafted with Jeffamine® M-2005 ; c) relaxometric radius R_{NMR} (nm, filled markers, solid lines) and saturation magnetisation M_S (empty markers, dotted lines) *vs.* temperature for USPIOs coated by Jeffamine® M-2005 (blue) and TEPSA only (red).

NMRD profiles, *i.e.* the curves of the longitudinal relaxivity r_1 *vs.* frequency ν were recorded before (Fig. 5a) and after (Fig. 5b) grafting of Jeffamine® M-2005 onto the TEPSA layer around the USPIOs at varying temperatures. These curves exhibited a profile typical for USPIOs, with a plateau at low frequency ascribed to the Néel fluctuations of the magnetic moments, a maximum at an intermediate frequency due to their orientation by the magnetic field (Curie mechanism) and a dropping down towards high frequencies usually interpreted as the absence of a "secular term" in the equation describing T_1 relaxation.[19] The whole curve $r_1(\nu)$ was shifted to lower values when temperature increased. The

View Article Online
DOI: 10.1039/C4NR07064J

predominant cause is the decrease of viscosity with temperature, accelerating the diffusion of water molecules around the USPIO and shortening the interaction between nuclear spins of protons and electronic spins of the USPIO. But the decrease became more abrupt when Jeffamine® M-2005 was grafted on top of the TEPSA layer, especially near the LCST between 20°C and 30°C.

A heuristic method to simplify the relaxation equations enables fitting such NMRD profiles $r_1(\nu)$: the resulting parameters are the relaxometric radius (R_{NMR}), the saturation magnetisation (M_S) of the Outer Sphere model equivalent to the iron oxide nanoparticles including their non-magnetic shell impermeable to water protons, and the diffusion constant of water molecules D.[19] Usually one takes $D=3\times10^{-9}$ $m^2\cdot s^{-1}$ in the model, which is the diffusion constant of water at 37°C. For the other temperatures studied here, D was set at values reported in literature.[24] Fig. 4c shows the plots of R_{NMR} and M_S deduced from the fits as a function of temperature. For USPIOs coated with a TEPSA layer only, the outer sphere radius and the magnetisation were found constant from 5°C to 50°C ($R_{NMR}\approx5.5$ nm and $M_S\approx52$ $A\cdot m^2\cdot kg^{-1}$), thereby confirming that the continuous lowering of the whole NMRD curve of the control TEPSA-coated USPIOs when temperature increases on Fig. 4a can be explained by the tabulated change of D with temperature, *i.e.* the viscosity effect.

On the contrary, the fitted parameters for USPIOs grafted with Jeffamine® M-2005 were found nearly constant only from 5°C to 20°C ($R_{NMR}\approx6$ nm and $M_S\approx46$ $A\cdot m^2\cdot kg^{-1}$), but then varied in opposite directions once the LCST of the chains was reached. Compared to nanoparticles coated by TEPSA only, those grafted with Jeffamine® M-2005 showed already below the LCST an increase of relaxometric radius by ~0.5 nm (as apparent from the slight shift of the curve towards lower ν) and a concomitant decrease of saturation magnetisation. These two observations can be ascribed to a non-magnetic layer wrapping the oxide cores, also impermeable to water protons, as sketched on Scheme 1. When passing the LCST of Jeffamine® M-2005, these two phenomena were amplified. The formation of a hydrophobic coating surrounding the USPIOs increases the minimal approach distance between the iron oxide surface and the water protons by ~1.8 nm, a quite reasonable size for polymer chains around 2400 $g\cdot mol^{-1}$ in the collapsed (bad solvent) or globular state.

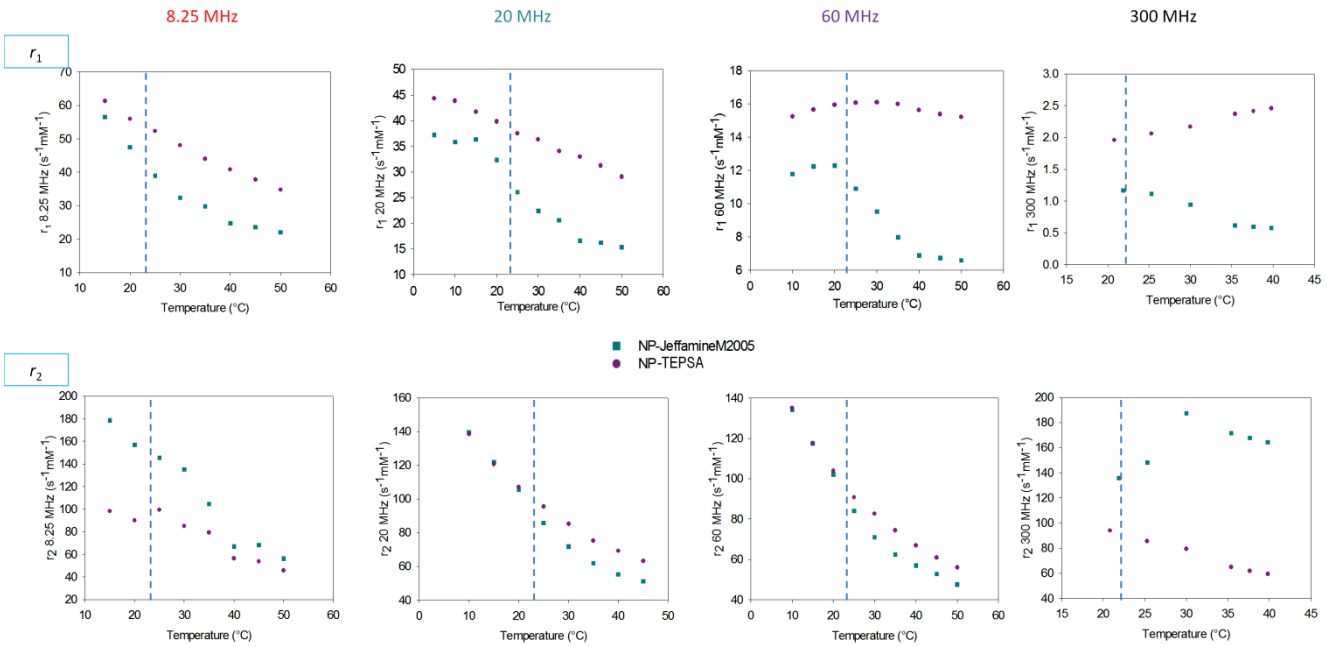

Fig. 6 Longitudial (r_1, top) and transverse (r_2, bottom) relaxivities at clinically relevant frequencies (from left to right: 8.25, 20, 60, and 300 MHz) for TEPSA-coated USPIOs (purple markers) and USPIOs grafted with Jeffamine® M-2005 (green markers) as a function of temperature from 10 to 50°C. The vertical dotted lines show the position of the LCST, concomitant with an inflection of the curve of r_2 *vs.* T.

Relaxivities r_1 and r_2 at frequencies of clinical MRI scanners (8.25, 20, 60 MHz) and at the highest field operated on humans (300 MHz) were plotted as a function of temperature (Fig. 6) for the USPIOs coated by TEPSA only and by Jeffamine® M-2005. Concerning longitudinal relaxation at these four frequencies, r_1 was lower for the polymer-coated USPIOs than for the ones coated by just a silane layer, in accordance with the presence of a barrier impermeable to water protons. For the TEPSA-coated USPIOs, the variation of r_1 with temperature was not the same for all the frequencies: being a decreasing function at 8.25 and 20 MHz, it was nearly flat at 60 MHz and became even a slightly increasing function at 300 MHz. Such a complex variation of r_1 of USPIOs, either increasing or decreasing with temperature, was described in a recent report, and ascribed to their variation of magnetic anisotropy depending upon their size and synthesis route.[23] On the contrary, r_2 was always a decreasing function of temperature at all frequencies for the TEPSA-coated USPIOs, in accordance with the Outer Sphere model predicting a scaling law with the square of the size and a prefactor inversely proportional to the diffusion constant of water as Eq (1), thus proportional to viscosity.[12] For the USPIOs grafted with Jeffamine® M-2005, the plot of longitudinal relaxativity *vs.* temperature showed a sigmoid shape with an inflection point near the LCST of the chains at all frequencies (this effect was even more pronounced when dividing

r_1 with by its value for the TEPSA-only control as on Fig. S8).

For the transverse relaxation of protons, r_2, the comparison between data of USPIOs coated by the polymer chains and of the uncoated ones led to a discrepancy between r_2 values obtained at 20 and 60 MHz on the one hand and at 8.25 and 300 MHz on the other hand: in the first case, the transverse relaxivity was identical for coated and uncoated USPIOs below the LCST, while above the LCST, r_2 decreased more rapidly than expected just by the temperature effect on water diffusivity (with TEPSA only). It should be noted that the direct temperature effect on the magnetic properties of the iron oxide can be ruled out to explain this decrease of r_2: the Langevin function indeed decreases slightly with temperature, but once temperature is expressed in Kelvin, this effect appears negligible compared to the effect of temperature on the solvent diffusivity, which is much more pronounced.

The steeper decrease of r_2 in the case of USPIOs coated by the polymer chains compared to simply a TEPSA silane layer can be interpreted by a fully hydrated polymer shell below the LCST, totally permeable to water, so that protons can reach the iron oxide surface where the field lines of the magnetic moment are strong (Scheme 1) just as in the uncoated case. Above the LCST, the polymer shell collapsed, leading to a lower r_2 due the decrease of magnetisation caused by the dilution of iron oxide by the non-magnetic layer (*i.e.* the same explanation as for the r_1 decrease). On the contrary, transverse relaxivities measured at 8.25 and 300 MHz were higher for the polymer-coated USPIOs than for uncoated ones at all temperatures. At 8.25 MHz, a plausible explanation is that the T_2-measuring sequences used on a MRI scanner did not have the same refocusing pulses as the CPMG spin echo method of a relaxometer, and thus measured the T_2* relaxation time rather than the pure T_2. At low temperature, the USPIOs coated by a swollen hydrophilic polymer shell exhibited the same r_2 as the uncoated ones (as measured at 20 and 60 MHz on relaxometers), but the magnetic field homogeneity was perturbed, as attested by r_2^* values measured on the 8.25 MHz MRI scanner much higher than r_2. Since the r_2 values at 300 MHz were measured on a NMR spectrometer and not a MRI scanner, the explanation must be different. In that case the much larger transverse relaxivity for the polymer-coated USPIOs compared to uncoated ones was ascribed to clustering by strong magnetic dipolar interactions, which causes a well-known increase of r_2. The electro-steric repulsion brought by Jeffamine® chains thus appeared to be less efficient to prevent USPIOs aggregation under a very high magnetic field than the electrostatic repulsion between highly negatively charged carboxylated silane layers.

The behaviour when temperature was increased also appeared to be different at low-field and at high-field. The intensity of magnetic dipolar interactions between clustered USPIOs varies indeed with the magnetic field value. At 8.25 MHz, the magnetic field was weak (B_0=0.194 T) and the magnetic moments were far from being saturated. In that case the collapse of chains above the LCST led to finite USPIOs clusters that must be around the same size as those measured by DLS in a zero magnetic field, D_h≈80 nm at 50°C. These clusters are also not very dense, as on the sketch deduced from the limited scattered intensity plotted on Fig. 4. The internal volume fraction of iron oxide is indeed one of the three control parameters determining the transverse relaxivity in addition to the size (R_{NMR} or D_h) and magnetisation.[12] For such tenuous aggregates above the LCST, Φ_{intra} must be much lower than for individually dispersed USPIOs. More precisely, Φ_{intra} varies like the number of USPIOs divided by the total volume, $\Phi_{intra} \sim N_{USPIO}/D_h^3$. The magnetisation M_S of the Outer Sphere equivalent to the aggregate being also proportional to Φ_{intra} (and to the specific magnetisation of the magnetic cores), the transverse relaxivity estimated by Eq. (1) varies as $r_2 \sim \Phi_{intra} \cdot D_h^2/D$ or equivalently $r_2 \sim N_{USPIO}/(D_h \cdot D)$. When temperature increased, both the aggregation number and the hydrodynamic diameter increased, but remained proportional to each other (Fig. 4). As a result, the clustering effect was too weak to enhance r_2, and the dominant effect was the increase of water diffusivity (D) with temperature as for individual TEPSA-coated USPIOs, explaining the decrease of r_2 and r_2* at 8.25 MHz (and up to 60 MHz). On the contrary, at 300 MHz the high magnetic field (B_0=7.05 T) induced intense magnetic dipolar interactions between aggregated USPIOs and amplified their clustering.[25] Their attraction and adhesion favoured by the dehydrated polymer layer at temperatures above the LCST increased both the size and the density of the clusters (thus their iron oxide load Φ_{intra}). This phenomenon explains why r_2 finally raised well above the values at 300 MHz of well dispersed uncoated USPIOs.

To conclude on this part, the behaviour of the USPIOs coated by thermo-sensitive poly(ether)amine chains with temperature and frequency appeared to be rather complex at first sight, but can still be interpreted by current models of r_1 and r_2 relaxivities. In practical, these variations of r_1 and r_2 with temperature can be turned into an advantage to efficiently modulate the contrast of MR images as a function of temperature, as shown in the next and final part of this study.

Properties as thermo-sensitive MRI contrast agent

To illustrate the interest of the thermo-sensitive polymer coated USPIOs, images of tubes filled with this sample and with the initial TEPSA-coated control were taken on a low-field (Fig. 7) and a high-field (Fig. 8) MRI scanners, the temperature being varied externally from 15 to 50°C with a circulating bath.

View Article Online
DOI: 10.1039/C4NR07064J

Cite this: DOI: 10.1039/c0xx00000x

www.rsc.org/xxxxxx

PAPER

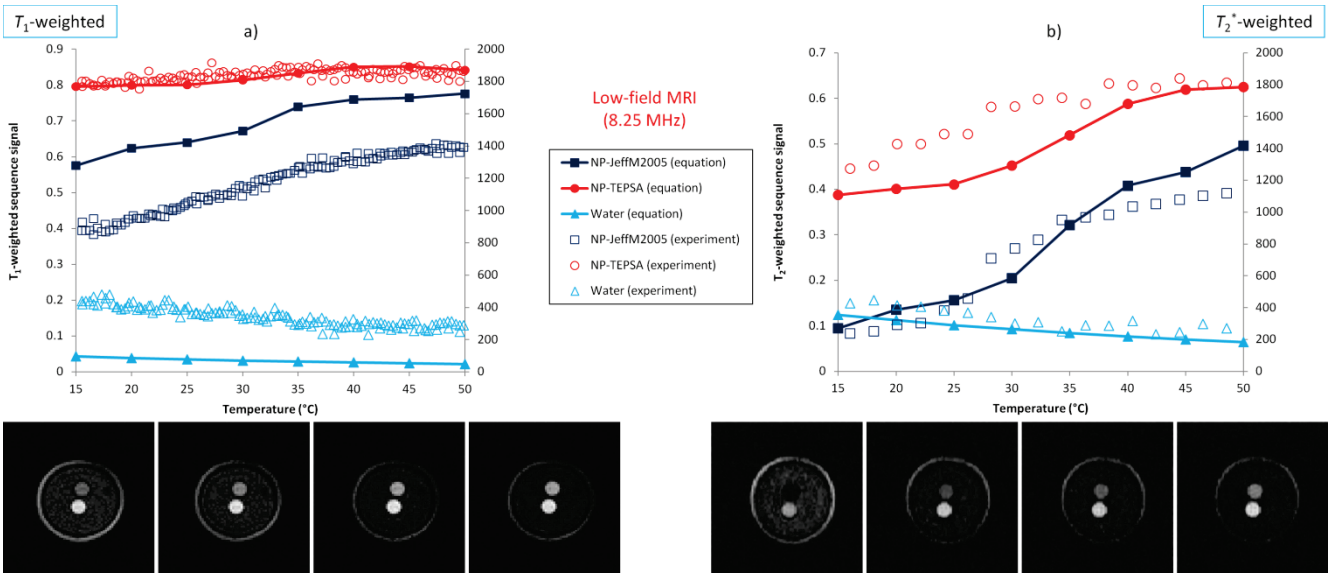

Fig. 7 Images taken on the low-field MRI scanner (8.25 MHz, 0.194 T) at increasing temperatures from 15 to 50°C with a) the T_1-weighted sequence (TR=100ms TE=2.8ms flip angle =70°) and b) the T_2*-weighted sequence (TR=300ms TE=12ms), 160×160 mm^2 field of view, 128×128 matrix, 7 mm slice thickness. The external light grey circle was ascribed to a perfusion MRI contrast of the water circulating in the double-wall of the glass chamber (diameter 50 mm) as compared to water at rest inside the chamber (dark grey). The tube at the upper position was filled with Jeffamine® M-2005 grafted USPIOs (1.1 mM_{Fe}) and the tube at the bottom position with the TEPSA-coated control (0.8 mM_{Fe}). The USPIOs exhibited a positive contrast (signal above the level of pure water) on all MR images except with the T_2*-weighting (b) for the USPIOs grafted with the chains below their LCST (15-25°C). The open markers show experimental signals. The closed markers and the solid lines represent theoretical predictions using Eq. (5) with the experimental values of T_1, T_2*, TE and TR. In the case of the Jeffamine® M-2005 grafted USPIOs, a linear regression of the experimental signal (normalised to the initial value at 15°C) *versus* temperature leads to slopes of +1.9%/°C and +16.6%/°C respectively for the T_1- and the T_2*-weighted sequences, with correlation coefficients R=0.98 and R=0.97, respectively. MRI cross-sections at the bottom line illustrate the variations of the signal plotted on the curves.

As the first striking feature, the low-field MR images (Fig. 7) showed a positive contrast brought by the TEPSA-coated USPIOs (increase of the signal level compared to pure water) with both the T_1-weighted and the T_2*-weighted sequence utilised. This can be easily interpreted by a r_2/r_1 ratio maintained at a low value ~1.5 at all temperatures (varying slightly in fact from 1.8 at 25°C to 1.3 at 45°C), demonstrating a perfect dispersion state of the USPIOs coated with the TEPSA silane. As comparison, USPIOs grafted with Jeffamine® M-2005 chains also exhibited positive contrast with the T_1-weighted sequence on the 8.25 MHz MRI scanner, but with a lower signal even at slightly higher iron concentration, as ascribed to a larger r_2/r_1 ratio. But as this ratio transited from a value 3.45±0.35 below the LCST to 2.7±0.2 above it (Table 2), the signal of a region of interest (ROI) centred on the sample tube increased from a level ~900 at 15°C to ~1400 at 50°C (Fig. 7a). Over the same temperature range, the control (TEPSA-NP) was kept at an almost constant level 1850±50. The thermo-sensitive signal of the Jeffamine® M-2005 coated USPIOs was even more spectacular with the T_2^*-weighted sequence (Fig. 7b). The sample exhibited indeed a contrast sign reversal at the exact LCST value, meaning that the curve of signal *vs.* temperature crossed the water baseline, nearly constant at 335±75.

In other words, the sample tube appeared at first on the images darker than pure water at low temperature, before becoming much brighter above the LCST of the polymer. The level measured in the ROI of the poly(ether)-coated USPIOs started from ~190 at 14°C and raised up to ~1100 at 50°C (Fig. 7b), meaning an increase by ~600% within 36°C temperature change. In the meanwhile, the control TEPSA-coated USPIOs showed only a moderate increase (by less than 40%) from ~1300 at 14°C to ~1800 at 50°C. To interpret such a really unusual behaviour compared to classical T_1 and T_2 MRI contrast agents, we computed the signal levels by the approximated solution of Bloch equations that is found in most MRI textbooks:

$$S_{\mathrm{MRI}} \propto \rho_{\mathrm{H}} \left(1 - e^{-TR/T_1}\right) \cdot e^{-TE/T_2} \qquad (5)$$

This estimate of the MRI signal is proportional to the volume density of the protons ρ_H and to the product of the longitudinal magnetisation recovered after the repetition time TR with the transverse magnetisation remaining after the echo time TE. The S_{MRI} calculated with experimental T_1 and T_2^* are represented for both pulse sequences by the filled data points on Fig. 7 and their numerical values are provided on Table 2 on an un-dimensioned scale (on which the signal of pure water is respectively 0.025 and 0.072 for the T_1 and the T_2^*-weighted sequences with T_1=T_2≈4s). The matching of the levels determined experimentally on the

View Article Online
DOI: 10.1039/C4NR07064J

different ROIs of the images by this rather crude theoretical formula is impressively good. In particular the relative values of the polymer-coated and the control USPIOs are well estimated at all temperatures, especially for the T_2^*-weighted sequence (Fig. 7b), the value of the polymer-coated USPIOs being slightly over-estimated by Eq. (5) for the T_1-weighted sequence (Fig. 7a). MRI cross-sections at the bottom of Figure 7 illustrate the variations of the signal plotted on the curves. For the two sequences (T_1- and T_2*-weighted), the bottom tube containing control TEPSA-NPs appears much brighter than the water around (T_1 effect) and shows a weak signal increase with temperature. On the opposite with the T_2*-weighted sequence only, the tube with Jeffamine® M-2005 coated NPs starts from a level darker than pure water, progressively rising up with temperature, crossing the water level near the LCST and then becoming much brighter at elevated temperatures. The water circulating in the double-wall of the water jacket containing the tubes appears always brighter than the water at rest just around the tubes, as ascribed to the migration velocity of the corresponding protons.

Table 2 Longitudinal (T_1) and transverse (T_2^*) proton relaxation times for Jeffamine® M-2005 grafted USPIOs (NP-Jeff2005) and a TEPSA-control (NP) enabling to compare the experimental signals of regions of interest on images on the low-field MRI scanner to the levels estimated from the approximated solution Eq. (5) of the Bloch equations with the echo time (*TE*) and the repetition time (*TR*) of the T_1-weighted and the T_2*-weighted spin echo sequences.

T (°C)	r_1 [a]	r_2^* [b] / r_1 [a]	T_1 (NP)	T_2^* (NP)	T_1 (NP-Jeff2005)	T_2^* (NP-Jeff2005)	T_1-weighted sequence on low-field MRI (*TR*=100ms *TE*=2.8ms flip angle =70°)				T_2*-weighted sequence on low-field MRI (*TR*=300ms *TE*=12ms)			
	NP-Jeff2005		0.8 mM_{Fe}		1.1 mM_{Fe}		NP 0.8 mM_{Fe}		NP-Jeff2005 1.1 mM_{Fe}		NP 0.8 mM_{Fe}		NP-Jeff2005 1.1 mM_{Fe}	
	$s^{-1}\cdot mM_{Fe}^{-1}$		ms	ms	ms	ms	S_{MRI} [c]	S_{MRI} [d]	S_{MRI} [c]	S_{MRI} [d]	S_{MRI} [c]	S_{MRI} [d]	S_{MRI} [c]	S_{MRI} [d]
15	56.4	3.2	20.2	12.7	16.0	5.1	1804	0.80	875	0.57	1300	0.39	213	0.09
20	47.5	3.2	22.1	13.1	19.0	6.0	1823	0.80	969	0.62	1428	0.40	292	0.13
25	39.0	3.6	23.7	13.5	23.1	6.5	1828	0.80	1053	0.64	1490	0.41	420	0.16
30	32.4	3.7	25.8	15.1	27.8	7.6	1846	0.81	1148	0.67	1663	0.45	772	0.20
35	29.7	2.9	28.2	18.3	30.3	10.6	1858	0.83	1269	0.74	1699	0.52	959	0.32
40	24.7	2.7	30.4	22.6	36.4	13.4	1856	0.85	1290	0.76	1796	0.59	1033	0.41
45	23.5	2.6	32.8	25.0	38.3	14.5	1880	0.85	1362	0.76	1819	0.62	1090	0.44
50	22.1	2.5	35.7	25.5	40.8	17.1	1899	0.84	1401	0.78	1814	0.62	1118	0.50

[a] measured at 8.25MHz by FFC; [b] measured on the low-field MRI at 0.194 T; [c] measured experimentally (arbitrary units); [d] calculated by Eq. (5) (no unit).

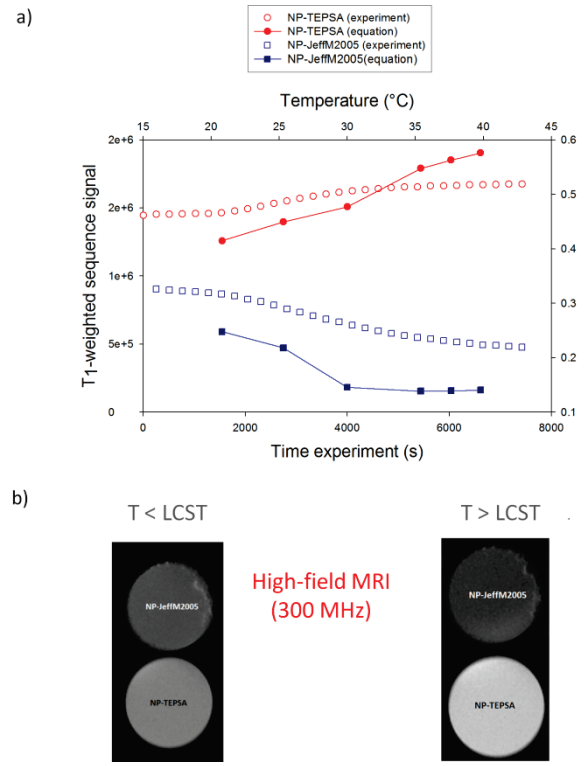

Fig. 8 a) Signal levels and b) images taken on the high-field MRI scanner (300 MHz, 7.05 T) at increasing temperatures from 21 to 40°C with a T_2*-weighted sequence (*TR*=1000ms *TE*=8.5ms), 25.6×25.6 mm^2 field of view, 256×256 matrix, and 2 mm slice thickness.

An analogous analysis was undergone for the high-field MRI images (Fig. 8). In that case the r_2/r_1 ratios were much higher, respectively ~48 for the TEPSA-NP and ~116 for the Jeffamine® M-2005 grafted USPIOs at 10°C. But whereas r_2/r_1 decreased to ~24 at 40°C for the control NP, it raised up to ~286 for the poly(ether)-coated USPIOs at 40°C, giving rise to an increase of the signal (positive contrast) in the former case and a decrease (negative contrast) in the latter case. This high r_2/r_1 was certainly ascribed to an important clustering of the Jeffamine® M-2005 grafted USPIOs under a magnetic field of 7.05 T. This means that a thicker and better repelling polymer corona would be absolutely necessary to achieve positive MRI contrast enhancement at such high field, especially in highly saline biological buffers. Since charged nanoparticles injected in blood plasma are immediately recognised by proteins of the immune system (opsonins),[26] the clinical translation to thermo-sensitive USPIOs providing positive MRI contrast *in vivo* would necessitate a pure steric repulsion (stealth effect), which is out of the scope of the present study.

Conclusions

Ultra-small superparamagnetic iron oxide (USPIO) nanoparticles were synthesised by alkaline coprecipitation in polyol, coated with a carboxy-silane and grafted by amide bond coupling with two commercial poly(ether)amines (Jeffamine® M-2005 and M-2070) of different compositions in EO and PO units. The aim was to decipher the influence of a hydrophilic or a hydrophobic shell wrapping the iron oxide core on longitudinal (r_1) and transverse (r_2) relaxivities, which determine their potential use as contrast agents for MRI. The relaxometric properties of USPIOs grafted with thermo-sensitive polymers were studied at four frequencies, on a low-field MRI scanner at 8.25 MHz, on a high-field MRI scanner and on a NMR spectrometer at 300 MHz, and on two relaxometers at frequencies 20 and 60 MHz close to those of 0.5 and 1.5 T clinical MRI scanners currently found in hospitals (21.3 and 63.9 MHz respectively). Except at 300 MHz, all the r_1 and r_2

View Article Online
DOI: 10.1039/C4NR07064J

values decreased markedly above the LCST of the chains, which could be reached only with Jeffamine® M-2005 since Jeffamine® M-2070 exhibited a much higher LCST. The relaxometric data were interpreted within the Outer Sphere model by the formation above the LCST of a hydrophobic coating wrapping the iron oxide cores, hence preventing water molecules to directly be in contact with the iron oxide surface, which lowered the interaction between the proton spins and the magnetic moments of the USPIOs. The r_2/r_1 ratios were kept at a low value (except at high magnetic field), demonstrating that the polymer corona was sufficiently repelling to prevent USPIOs' aggregation in water. This characteristics of the NMRD profiles were turned into positive contrast enhancement on the low-field MRI scanner, not only for the T_1-weighted sequence, but also for the T_2*-weighted one, once the LCST was reached. In that case, the signal measured on a sample tube at 1.1 mM_{Fe} was found nearly linear with temperature in the 15–50°C range. This finding offers the possibility of non-invasive detection by MRI of localised temperature changes or gradients within the body, for instance during any kind of hyperthermia treatment for cancer catabolism.

There are three different ways to map temperature by MRI.[27] The first idea was to use the Arrhenius-type law of the spin-lattice relaxation time T_1 of water and tissues *vs.* temperature,[28] but it suffers from inaccuracy due to weak dependence (~1% per °C) and poor linearity of the signal (linear regression coefficient R<0.8).[27] Therefore a more sensitive alternative was proposed,[29] relying on the measurement by diffusion-weighted MRI of the diffusion coefficient of water molecules, which varies by 2.4% per °C. However D-weighted MRI is delicate and prone to body motion artefacts.[27] This is why the current method implemented on most medical MRI scanners is signal phase mapping, which converts the chemical shift of proton resonance frequency (PRF), that varies by -0.01 ppm/°C, into a phase difference changing by ~10° per °C in a perfect linear manner (R~0.99).[30] Both diffusion MRI and phase mapping lead to a precision of ±0.5°C, but these two techniques require rather complex algorithms to get rid of artefacts such as body motions and to convert the signal into temperature information. Other methods using thermo-sensitive liposomes loaded with paramagnetic ions[31,32] or chemical shift agents[33] were described. But the signal was not linear and varied abruptly near the melting temperature of the lipids, so that their response was rather on/off than a graduated scale to build a thermometer. In the present study, the signal of the poly(ether)-coated USPIOs with the T_2*-weighted sequence on the low-field MRI scanner (Fig. 7b) varied by 16.6% per °C (or by 100% every 6°C), so that the raw signal of the image (without any data treatment) increased by 600% when temperature was increased from 14-15°C to 48-50°C with a linear regression coefficient R~0.97 and perfect reversibility when temperature was decreased back. This study proved the concept *in vitro* (*i.e.* in tubes) of MRI thermo-sensitive positive contrast agents with a sensitivity (in % variation/°C) potentially one order of magnitude higher than with the current methods and a good linearity of signal (R~0.97) in the medical temperature range, which are prerequisites to build an absolute thermometer.

The next step in further studies will be to modify these temperature-responsive positive MRI contrast agents so that they can work also *in vivo*: in particular the challenge will consist in improving the stealth behaviour of the polymer corona so that it efficiently prevents the aggregation of the USPIOs in high salinity buffers supplemented with blood plasma proteins, while maintaining temperature responsiveness of the coating. Bio-polymers with some characteristic transition temperature (e.g. secondary structure melting) might be the best candidates to be grafted onto USPIOs and to achieve the *in vivo* translation of the paradigm evidenced by the present *in vitro* study.

Abbreviations

EO, ethylene oxide; PO, propylene oxide; LCST, lower critical solution temperature; NP, nanoparticle; USPIO, ultra-small superparamagnetic iron oxide nanoparticle; DLS, dynamic light scattering; NMR, nuclear magnetic resonance; r_2, transverse relaxivity; r_1, longitudinal relaxivity; T_2, transverse relaxation time; T_1, longitudinal relaxation time; MRI, magnetic resonance imaging; D_h, hydrodynamic diameter; APTS , (3-aminopropyl)triethoxysilane; R_{NMR}, distance of closest approach between the water protons and the superparamagnetic particle; Φ_{intra}, intra-particle volume fraction of magnetic materials; M_S, magnetisation at saturation; γ, proton gyromagnetic factor; μ_0, magnetic permeability of vacuum; D, diffusion constant of water molecules; v_{mol}, specific volume of the magnetic material; DI, de-ionized; TEPSA, 3-triethoxysilylpropyl succinic anhydride; PDI, polydispersity index; PALS, phase analysis light scattering; TEM, transmission electron microscopy; IR, infrared; NMRD, nuclear magnetic relaxation dispersion; TGA, thermogravimetric analysis; CPMG, Carr Purcell Meiboom Gill; *TR*, repetition time; *TE*, echo time; PZC, point of zero charge; v, frequency; ROI, region of interest; EDC, 1-ethyl-3-(3-dimethylaminopropyl)carbodiimide.

Notes and references

[a] *Department of General, Organic and Biomedical Chemistry, NMR and Molecular Imaging Laboratory, University of Mons, 19 avenue Maistriau, B-7000 Mons, Belgium. Fax: +32-65-373520; Tel: +32-65-373525; E-mail: sophie.laurent@umons.ac.be*
[b] *Center for Microscopy and Molecular Imaging, 8 rue Adrienne Bolland, B-6041 Charleroi, Belgium*
[c] *Laboratoire de Chimie des Polymères Organiques, UMR5629 CNRS / Université de Bordeaux, ENSCBP 16 avenue Pey Berland F-33607 Pessac, France. Fax: +33-5-4000-8487; Tel: +33-5-4000-3695; E-mail: olivier.sandre@enscbp.fr*
[d] *Résonance Magnétique des Systèmes Biologiques, UMR 5536 CNRS / Université de Bordeaux 146, rue Léo Saignat, F-33076, Bordeaux France*

† Electronic Supplementary Information (ESI) available: Fig. S1: a) ^{1}H NMR spectra *vs.* temperature for Jeffamine® M-2005, b) and M-2070 at 30 $mg{\cdot}mL^{-1}$ in D_2O; Fig. S2: FT-IR spectra of iron oxide nanoparticles a) just after coprecipitation, and b) after coating with TEPSA; Fig. S3: Thermogravimetric analyses (TGA) of USPIOs silanized by TEPSA (red curve), and after coupling with Jeffamine® M-2005 (green curve) and M-2070 (blue curve); Fig. S4: FT-IR spectra a) of the difference between the normalised spectra of USPIOs coated with TEPSA before and after grafting of Jeffamine® M-2005, and b) of Jeffamine® M-2005 alone; Fig. S5: FT-IR spectra a) of the difference between the normalised spectra of USPIOs coated with TEPSA before and after grafting of Jeffamine® M-2070, and b) of Jeffamine® M-2070 alone; Fig. S6: NMRD profiles of the longitudinal relaxivity *vs.* proton Larmor frequency for a) TEPSA-coated USPIOs, and b) USPIOs grafted with Jeffamine® M-2070 as function of temperature; Fig. S7: a) Outer sphere radius R_{NMR} and saturation magnetisation M_S *vs.* temperature for USPIOs coated by Jeffamine® M-2070 (green markers) and TEPSA only (purple markers); Fig. S8: longitudial r_1 and transverse r_2 relaxivities of USPIOs grafted with Jeffamine® M-2005, normalised by the corresponding r_1 or r_2 of TEPSA-coated USPIOs, as function of temperature from 10 to 50°C, for clinically relevant frequencies: 8.25, 20, 60, and 300 MHz. Movie1: 8.25 MHz MR image of Jeffamine® M-2005 NP-coated and NP-TEPSA control tubes during a temperature cycle with the T_1-weighted sequence. Movie2: 8.25

MHz MR image of Jeffamine® M-2005 NP-coated and NP-TEPSA control tubes during a temperature cycle with the T_2*-weighted sequence
See DOI: 10.1039/b000000x/

‡ The authors are grateful to Dr. Laetitia Mespouille and Dr Alain Roch for helpful discussions. The authors also thank the laboratory of Polymeric and composite Materials (Prof P. Dubois) of the University of Mons for additional TGA analysis studies. This work was performed with the financial support of the FNRS, the CNRS (MI G3N "NanoBlast"), the ARC program, the ENCITE program and the RW (AGECO project), the Interuniversity Attraction Poles of the Belgian Federal Science Policy Office, the Agence Nationale de la Recherche ANR-13-BS08-0017 and the European Commission under the seventh framework within the frame of ESF RNP "Precision Polymer Materials" P2M, and COST actions TD1004, TD1007, TD1402 and CM1006. The authors also would like to acknowledge the Center for Microscopy and Molecular Imaging (CMMI, supported by the European Regional Development Fund and Wallonia).

Author Contributions

The manuscript was written by A. H., S. L. and O. S. through contributions of all authors. A.H., D.S. and S.L. synthesized the iron oxide cores and performed the TEPSA silane grafting. A. H., J. T., C. B., O. S. and S. L. designed the polymer grafting procedure. A.H. did the polymer grafting and all the physicochemical characterisations. A. H., L. V. E, R. N. M and S.L. designed and performed the proton relaxometry and high field MRI experiments. O. S., A. T., P. M. and S. M. performed and interpreted the low field MRI experiments. All authors have given approval to the final version of the manuscript.

1 S. Laurent, J. Bridot, L. Vander Elst, and R. N. Muller, *Future Med. Chem.*, 2010, **2**, 427-449 ; S. Laurent, D. Forge, M. Port, A. Roch, C. Robic, L. Vander Elst, and R. N. Muller, *Chem. Rev.*, 2008, **108**, 2064-2110; A. K. Gupta and M. Gupta, *Biomat.*, 2005, **26**, 3995-4021 ; Q. A. Pankhurst, J. Connolly, S. K. Jones, and J. Dobson, *J. Phys.* D*: Appl. Phys.*, 2003, **36**, R167-R181; S. Mornet, S. Vasseur, F. Grasset, E. Duguet, *J. Mater. Chem.*, 2004, **14**, 2161-2175; Q. A. Pankhurst, N. K. T. Thanh, S. K. Jones, and J. Dobson, *J. Phys.* D*: Appl. Phys.*, 2009, **42**, 224001.

2 S. Laurent, S. Boutry. I. Mahieu, L. Vander Elst, and R. N. Muller, *Cur. Med. Chem.*, 2009, **16**, 4712-4727; S. Laurent, L. Vander Elst, and R. N. Muller, "Encyclopedia of Magnetic Resonance", R. K. Harris and R. Wasylishen Eds., John Wiley: Chichester 2009; Y. Gossuin, P. Gillis, A. Hocq, Q. L. Vuong, and A. Roch, *WIREs Nanomed. Nanobiotechnol.*, 2009, **1**, 299-310.

3 U. I. Tromsdorf, O. T. Bruns, S. C. Salmen, U. Beisiegel, and H. Weller, *Nano Letters*, 2009, **9**, 4434-4440.

4 T. Ninjbadgar, D. F. Brougham, *Adv. Funct. Mater.*, 2011, **21**, 4769-4775.

5 T. Borase, T. Ninjbadgar, A. Kapetanakis, S. Roche, R. O'Connor, C. Kerskens, A. Heise, and D. F. Brougham, *Angew. Chem. Int. Ed.*, 2013, **52**, 3164-3167

6 Z. Xu, Q. Liu, J. A. Finch, *Appl. Surf. Sci.*, 1997, **120**, 269-278 ; M. Yamaura, R. L. Camilo, L. C. Sampaio, M. A. Macêdo, M. Nakamura, H. E. Toma, *J. Magn. Magn. Mater.*, 2004, **279**, 210-217; S. Mornet, J. Portier, E. Duguet, *J. Magn. Magn. Mater.*, 2005, **293**, 127-134; A. del Campo, T. Sen, J.-P. Lellouche, I. Bruce, *J. Magn. Magn. Mater.*, 2005, **293**, 33-40; I. J. Bruce, T. Sen, *Langmuir*, 2005, **21**, 7029-7035; W. Wu, Q. He, C. Jiang, *Nanoscale Res. Lett.*, 2008, **3**, 397-415; F. Galeotti, F. Bertini, G. Scavia, A. Bolognesi, *J. Coll. & Interf. Sci.*, 2011, **360**, 540-547; N. Arsalania, H. Fattahia, S. Laurent, C. Burtea, L. Vander Elst, R. N. Muller, *Contr. Media Mol. Imag.*, 2012, **7**, 185-194.

7 R. De Palma, S. Peeters, M. J. Van Bael, H. Van den Rul, K. Bonroy, W. Laureyn, J. Mullens, G. Borghs, and G. Maes, *Chem. Mater.* 2007, **19**, 1821-1831; J. Trekker, K. Jans, H. Damm, D. Mertens, T. Nuytten, J. Vanacken, V. Moshchalkov, J. D'Haen, T. Stakenborg, W. Van Roy, U. Himmelreich and L. Lagae, *IEEE Trans. Magn.*, 2013, **49**, 219-226.

8 Y. Sun, X. Ding, Z. Zheng, X. Cheng, X. Hu, and Y. Peng, *Eur. Polym. J.*, 2007, **43**, 762-772.

9 D. Forge, S. Laurent, Y. Gossuin, A. Roch, L. Vander Elst, R. N. Muller, *J. Magn. Magn. Mater.*, 2011, **323**, 410-415.

10 S. Pinho, S. Laurent, J. Rocha, A. Roch, M.-H. Delville, L. Carlos, L. Vander Elst, R. N. Muller, C. Geraldes, *J. Phys. Chem.* C, 2012, **116**, 2285-2291.

11 C. Paquet, H. W. de Haan, D. M. Leek, H.-Y. Lin, B. Xiang, G. Tian, A. Kell, and B. Simard, *ACS Nano*, 2011, **5**, 3104-3312; H. W. de Haan, C. Paquet, *Magn. Res. Med.*, 2011, **66**, 1759-1766; J. S. Riffle, N. Pothayee, S. Balasubramanian, N. Pothayee, N. Jain, N. Hu, Y. Lin, R. M. Davis, N. Sriranganathan, and A. P. Koretsky, *J. Mater. Chem.* B, 2013, **1**, 1142-1149.

12 Q. L. Vuong, J.-F. Berret, J. Fresnais, Y. Gossuin, and O. Sandre, *Adv. Health. Mat.*, 2012, **1**, 502-512.

13 D. Schmaljohann, *Adv. Drug Del. Rev.*, 2006, **58**, 1655-1670; A. E. Smith, X. Xu, C. L. McCormick, *Prog. Polym. Sci.*, 2010, **35**, 45-93.

14 W. Agut, A. Brûlet, D. Taton, and S. Lecommandoux, *Langmuir*, 2007, **23**, 11526-11533.

15 S. Belbekhouche, G. Ali, V. Dulong, L. Picton, and D. Le Cerf, *Carboh. Polym.*, 2011, **86**, 304-312.

16 S. Louguet, B. Rousseau, R. Epherre, N. Guidolin, G. Goglio, S. Mornet, E. Duguet, S. Lecommandoux, and C. Schatz, *Polym. Chem.*, 2012, **3**, 1408-1417.

17 F. Azzam, L. Heux, J.-L. Putaux, and B. Jean, *Biomacromol.*, 2010, **11**, 3652-1659.

18 D. Forge, A. Roch, S. Laurent, H. Tellez, Y. Gossuin, F. Renaux, L. Vander Elst, and R. N. Muller, *J. Phys. Chem.* C, 2008, **112**, 19178-19185.

19 A. Roch, R. N. Muller, P. Gillis, *J. Chem. Phys.*, 1999, **110**, 5403-5411; P. Gillis, A. Roch, R. A. Brooks, *J. Mag. Res.*, 1999, **137**, 402-407.

20 S. Boutry, D. Forge, C. Burtea, I. Mahieu, O. Murariu, S. Laurent, L. V. Elst, and R. N. Muller, *Contr. Media Mol. Imag.*, 2009, **4**, 299-304.

21 M. V. Deshmukh, A.A. Vaidya, M. G. Kulkarni, P. R. Rajamohanan, and S. Ganapathy, *Polym.* , 2000, **41**, 7951-7960.

22 S. Balasubramaniam, N. Pothayee, Y. Lin, M. House, R. C. Woodward, T. G. St. Pierre, R. M. Davis, and J. S. Riffle, *Chem. Mat.*, 2011, **23**, 3348-3356.

23 E. D. Smolensky, H-Y. E. Park, Y. Zhou, G. A. Rolla, M. Marjanska, M. Botta, and V. C. Pierre, *J. Mater. Chem.* B, 2013, **1**, 2818-2828.

24 M. Holz, S. R. Heil, and A. Sacco, *Phys. Chem. Chem. Phys.*, 2000, **2**, 4740-4742.

25 N.J. Darton, A. J. Sederman, A. Ionescu, C. Ducati, R. C. Darton, L. F. Gladden, N. K. Slater, *Nanotechnology*, 2008, **19**, 395102-395106.

26 M. P. Monopoli, D. Walczyk, A. Campbell, G. Elia, I. Lynch, F. Baldelli Bombelli, K. A. Dawson, *J. Am. Chem. Soc.*, 2011, **133**, 2525-2534.

27 W. Wlodarczyk, R. Boroschewski, M. Hentschel, P. Wust, G. Monich, R. Felix, *J. Magn. Reson. Imag.*, 1998, **8**, 165-174; B. Quesson, J. A. de Zwart, C. T.W. Moonen, *J. Magn. Res. Imag.*, 2000, **12**, 525-533.

28 D. L. Parker, V. Smith, P. Sherldon, L.E. Crooks, L. Fussel, *Med. Phys.*, 1983, 10, 321-325.

29 D. Le Bihan, J. Delannoy, R. L. Levin, *Radiology* 1989, **171**, 853-857.

30 Y. Ishihara, A. Calderon, H. Watanabe, *Magn. Res. Med.,* 1995, **34**, 814-823; J. de Poorter, *Magn. Res. Med.* 1995, **34**, 359; K. K. Vigen, B. L. Daniel, J. M. Pauly, K. Butts, *Magn. Reson. Med.,* 2003, **50**, 1003-1010; V. Rieke, K. K. Vigen, G. Sommer, B. L. Daniel, J. M. Pauly, K. Butts, *Magn. Reson. Med.*, 2004, **51**, 1223-1231; B. Denis de Senneville, B. Quesson, C. T. W. Moonen, *Int. J. Hyperthermia*, 2005, **21**, 515-531; K. Kuroda, D. Kokuryo, E. Kumamoto, K. Suzuki, Y. Matsuoka, B. Keserci, *Magn. Reson. Med.*, 2006, **56**, 835-843.

31 R. Salomir, J. Palussière, S. L. Fossheim, A. Rogstad, U. N. Wiggen, N. Grenier, C. T. W Moonen, *J. Magn. Res. Imaging* 2005, **22**, 534-540; C. Bos, M. Lepetit-Coiffé, B. Quesson, C. T. W. Moonen, *Magn. Res. Med.*, 2005, 54, 1020-1024.

32 R. M. Davis, B. L. Viglianti, P. Yarmolenko, J-Y. Park, P. Stauffer, D. Needham, M. W. Dewhirst, *Int. J. Hyperthermia*, 2013, **29**, 569-581.

View Article Online
DOI: 10.1039/C4NR07064J

33 S. Langereis, J. Keupp, J. L. J. van Velthoven, I. H. C. de Roos, D. Burdinski, J. A. Pikkemaat, and H. Grüll, J. Am. Chem. Soc., 2009, 131, 1380-1381.